

Contents lists available at ScienceDirect

Acta Materialia

journal homepage: www.elsevier.com/locate/actamat



Full length article

Resonant interaction between phonons and PbTe/PbSe (001) misfit dislocation networks



Yang Li^{a,*}, Zexi Zheng^b, Adrian Diaz^c, Simon R. Phillpot^d, David L. McDowell^{e,f}, Youping Chen^a

- ^a Department of Mechanical and Aerospace Engineering, University of Florida, Gainesville, FL 32611, USA
- ^b College of Mechanical Engineering, University of Shanghai for Science and Technology, Shanghai 200093, China
- ^cX-Computational Physics Division, Los Alamos National Laboratory, P.O. Box 1663, Los Alamos, NM, USA
- ^d Department of Materials Science and Engineering, University of Florida, Gainesville, FL 32611, USA
- ^e Woodruff School of Mechanical Engineering, Georgia Institute of Technology, Atlanta, GA 30332, USA
- ^fSchool of Materials Science and Engineering, Georgia Institute of Technology, Atlanta, GA 30332, USA

ARTICLE INFO

ABSTRACT

Article history:
Received 11 January 2022
Revised 29 June 2022
Accepted 2 July 2022
Available online 3 July 2022

This work aims at a quantitative and mechanistic understanding of the dynamic process of the phonondislocation interaction in PbTe/PbSe (001) heterostructures using the Concurrent Atomistic-Continuum (CAC) method as the simulation tool. The misfit dislocation network and the atomic-scale dislocation core structure obtained in the simulations are found to agree reasonably well with the experimental observations of the PbTe/PbSe (001) interface. Through visualizing the dynamic interaction between phonons and dislocations, as well as quantifying the dislocation vibration amplitude, the phonon energy transmission, and the thermal resistance of the misfit interfaces, this work has illustrated and quantified two mechanisms for phonon-dislocation interaction: (1) phonon scattering by the strain field of dislocations, and (2) phonon scattering by dislocations that vibrate via the local modes of a dislocation network; the latter, leads to resonant phonon-dislocation interaction, which is manifested as local maxima of out-of-phase vibration of the atoms on the two sides of the slip plane, leading to local minima of the energy transmission in the heterostructure that contains one interface. The local vibrational modes are found to be excited only by shear stress induced by transverse phonons. Among various resonant modes, the one with the lowest frequency has the strongest effect. This work has also demonstrated the collective motion of dislocations under ultrafast phonon pulses. In addition, the dynamic properties of the misfit dislocation network localized within one interface are found to be significantly altered by the presence of misfit dislocations at other interfaces, thus further confirming the cooperative dynamic nature of the motion of dislocations and phonons.

© 2022 Acta Materialia Inc. Published by Elsevier Ltd. All rights reserved.

1. Introduction

Dislocations are ubiquitous crystallographic defects that form during materials syntheses or during thermal or mechanical processes. Dynamics of atoms in crystals are inevitably influenced by the interaction between dislocations and phonons. This interaction is the basis for the microscopic description and understanding of many important material phenomena such as plastic flow, materials damping, and thermal resistance. Our understanding of this interaction, however, is very limited.

In his attempt to explain the observed damping of mechanical vibrations in single crystals, Eshelby [1] described two mech-

* Corresponding author.

E-mail address: yangli1991@ufl.edu (Y. Li).

anisms: "damping due to the interaction between the vibrational stresses and the stresses surrounding *stationary* dislocations, and damping due to the emission of elastic waves from an *oscillating* dislocation". Eshelby observed that "the effect arising from stationary dislocations is inadequate to explain the damping observed in single crystals", while "the effect of moving dislocations seems capable of explaining the right order of magnitude". In 1951 Nabarro [2] noticed that "a sound wave passing near the dislocation is scattered"; by adapting Peierls's dislocation model to dynamical problems, Nabarro explained the two mechanisms from the viewpoint of phonon (wave) scattering: (1) static scattering of phonons by "the inhomogeneous strain field of a stationary dislocation", and (2) dynamic scattering by dislocations "that move (oscillate) under the influence of the sound wave" [2]. Nabarro envisaged that "a dislocation re-radiates elastic waves as it oscillates" and that a

"stationary dislocation produces no large-angle scattering of long waves" [2]. Using the re-radiation scattering cross-section calculated by Nabarro, Granato showed that the dynamic scattering by vibrating (fluttering) dislocations is much greater than the static scattering [3].

These two different mechanisms seem to lead to significantly different phonon transport behavior. In 1959, thermal conductivity measurements of compressed LiF at low temperatures by Sproull et al. [4] suggested that dislocations have more than 1000 times greater effect on phonon scattering than that predicted by Klemens's theory of stationary dislocations [5]. Later, Anderson and co-workers [6,7] measured the thermal conductivities of singlecrystal LiF at ~1 K before and after plastic deformation, respectively, as well as after γ irradiation of the plastically deformed LiF. γ irradiation does not remove dislocations but pins down mobile dislocations, and hence renders mobile dislocations sessile, thus making it possible to quantify the contribution of mobile dislocations to thermal resistance. Their measurements established: (1) the scattering of phonons by pinned (stationary) dislocations or point defects is very weak, and (2) there is a large decrease in the thermal conductivity of LiF after plastic deformation, and this decrease is due to dynamic, rather than static, scattering by disloca-

The most widely used theory to quantitatively describe the dynamic scattering is the elastic string model first developed by Koehler [8], built on the analogy between the vibration of a pinned dislocation line segment and the vibration of a string [8]. According to the string model, "a pinned dislocation shall resonate at certain frequencies" [8-10]. A generalization of Koehler's string model is the Granato-Lucke [9] model, which predicts that a dislocation line stretched between pinning points a distance L apart exhibits a resonant frequency inversely proportional to L. However, the string model does not quantitatively explain the thermal conductivities measured by Anderson and coworkers, while the experiments were quantitatively reproduced by many others. This led to various conjectures on the phonon-dislocation interaction mechanism. For example, Taylor and coworkers experimentally observed a strong decrease in thermal conductivity at low temperatures after plastic deformation in LiF, as well as in KCl, NaCl, and NaF [11]. They also found a large difference in the thermal conductivities between plastically deformed LiF by bending and that by shearing. The discrepancy between theory and experiment was thus suggested to be due to "cooperative scattering by non-randomly distributed dislocations" [11]. Meantime, Kneezel and Granato [12] conducted a comprehensive theoretical investigation into possible factors that might contribute to the discrepancy between the string model and experimental measurements. Their study, however, did not resolve the problem, and they concluded: "independently vibrating dislocations are not the important phonon scatterers" [12].

There are two possible causes for the failure of the string model in reproducing experimental measurements: (1) it ignores dislocation core structures, and hence cannot provide an accurate description of the dynamic interaction between phonons and dislocations, and (2) it ignores the interaction between dislocations, and consequently it cannot account for cooperative phonon scattering by multiple dislocations. Phonon scattering by dislocations in real materials is probably too complex to be described by simple analytical models or investigated by purely nanoscale computational methods. To gain insights into the problem, a computational approach needs to simultaneously reproduce the atomic-scale dislocation core structures, the long-range interaction between dislocations, and the phonon-dislocation interaction covering a wide phonon wavelength range, since at low temperatures the low-frequency long-wavelength phonons are the major heat carriers and may be more strongly scattered by mobile dislocations [13]. The molecular dynamics (MD) simulation method has been used to study the effect of dislocations on phonon transport [14–16]. However, MD has not been useful for studies of long-wavelength phonons because it cannot capture phonons with wavelengths larger than the periodic simulation box, and yet long-wavelength phonons are most important in the dynamic interaction between phonons and dislocations. The concurrent atomistic-continuum (CAC) [17–19] method has the capability of addressing all of the issues mentioned above.

This work aims to investigate the dynamic process of phonon scattering on vibrating and interacting dislocations. We select the misfit dislocation networks in PbTe/PbSe (001) interface for this study because, (1) similar to that in alkali halides, a strong reduction of thermal conductivity by dislocations has also been observed in lead chalcogenides such as PbS at low temperatures [20]; (2) dislocations in PbTe and PbSe systems are highly mobile and there exists well-documented experimental data concerning the dislocation networks at the PbTe/PbSe (001) heterointerface [21,22]; (3) there are reasonably well-developed interatomic potentials for the PbTe/PbSe system [23,24]; and (4) PbTe/PbSe heterostructures represent one of most important thermoelectric materials systems [25,26]. We employ the concurrent atomisticcontinuum (CAC) [19] method for the simulations of misfit dislocation networks in PbTe/PbSe (001) heterostructures and subsequently the interactions between the dislocations, interfaces, and phonons in the heterostructures, with phonon wavelength ranging from the atomic to the submicron scale. CAC is an atomistic method that employs a concurrent two-level structural description of crystalline materials: a continuous description of the structure of crystals at the unit cell level, and a discrete description of the organization of atoms within each unit cell [19]. It extends the applicability of atomic-interaction-based computational methods from the nanoscale to the micro- or meso-scale by solving the exact atomic trajectories, as molecular dynamics (MD), in structurally disordered or other critical regions, while simultaneously solving interpolated atomic positions utilizing the continuous distribution of unit cells in ordered crystalline region. Both the atomically resolved and the coarse-grained regions in the computer models are governed under the same set of governing equations using a single interatomic potential. Defect structures associated with heterointerfaces, dynamics of dislocations, and the collective interaction between dislocations, interfaces, and phonons all emerge in the simulation with no empirical rules, parameters, or presumed phonon transport mechanisms other than the interatomic potential.

This paper is organized as follows. After this Introduction, in Section 2 we present the computational method and the obtained misfit dislocation networks in PbTe/PbSe (001) heterostructures containing one and two interfaces, respectively. In Section 3, we report and analyze the simulation results of phonon-dislocation interactions in PbTe/PbSe (001) heterostructures, quantify the mechanisms for phonon-dislocation interactions, and demonstrate the collective motion of misfit dislocation networks. This paper concludes with a brief summary and discussions in Section 4.

2. Computational method and misfit dislocation networks in PbTe/PbSe (001) heterostructures

2.1. CAC computational method

The CAC method builds on the formulation that extends Irving and Kirkwood's statistical mechanical theory of transport processes for homogenized systems to a concurrent atomistic-continuum representation of non-equilibrium processes in general crystalline materials. The local densities of conserved quantities are defined per unit-cell volume per time-step interval [19,27,28], and consequently these densities are continuously distributed in equilibrium or steady-state crystalline materials, while fluxes are obtained as surface densities that satisfy the conservation laws without the

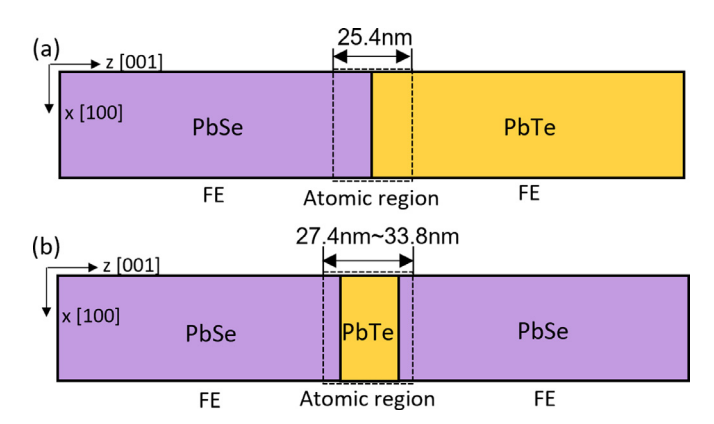


Fig. 1. 2D schematics of PbTe/PbSe heterostructures with (a) one interface, and (b) two interfaces; the crystallographic orientation is x//[100], y//[010], and z//[001]. Both models have the dimensions of 69 nm \times 69 nm \times 1.3 μ m.

need of being continuous [19,27-30]. To facilitate numerical implementation using the finite element method, the CAC integral form of the conservation equation for linear momentum has been recast in terms of internal force density, $\mathbf{f}_{\alpha}^{\text{int}}(\mathbf{x},t)$, and temperature gradient as [19]

$$\rho_{\alpha} \dot{\mathbf{v}}_{\alpha} = \mathbf{f}_{\alpha}^{\text{int}}(\mathbf{x}, t) + \mathbf{f}_{\alpha}^{T}(\mathbf{x}, t),$$
where
$$\frac{1}{\Delta t} \int_{0}^{\Delta t} \mathbf{f}_{\alpha}^{T}(\mathbf{x}, t + \tau) d\tau = \lambda \nabla_{\mathbf{x}} T(\mathbf{x}, t),$$
(1)

where $\rho_{\alpha}\mathbf{v}_{\alpha}$ represents the density of linear momentum of α -th atom in the primitive unit cell located at point \mathbf{x} ; $\mathbf{f}_{\alpha}^{\text{int}}$ is the internal force density per unit-cell volume; Δt is the time-step interval, as the equation of motion is solved in discrete time steps; \mathbf{f}_{α}^{T} is related to the kinetic part of stress due to fine-scale thermal fluctuations and has the effect of an external force; T is the kinetic temperature and is related to the kinetic stress; and λ is a constant determined by the mesh size in the finite element (FE) implementation. Eq. (1) is actually a multi-time scale representation. For non-equilibrium processes, $\nabla_{\mathbf{x}}T$ is a constant within an element if the usual tri-linear shape functions are used; \mathbf{f}_{α}^{T} can then be modeled as a body force with a constant mean in each element along with periodic or random fluctuations in time with the frequencies of the phonons that are cut off by the FE shape functions. Please see ref. [19] for more details.

The CAC balance equation of linear momentum has been implemented in the LAMMPS codebase using a modified finite element method [31]. Its accuracy and efficiency have been tested through one-to-one comparisons with MD for simulations of crack initiation and branching [32,33], phase transitions [34], dislocation nucleation [35–38], dislocation loop formations [39–42], and interactions with other defects [43–49], or phonon-dislocation [50,51], phonon-interface [52], and phonon-internal surface interactions [53].

In this work, two sets of CAC models of the PbTe/PbSe heterostructures are built. One model contains one PbTe/PbSe (001) interface and the others have two PbTe/PbSe (001) interfaces, as shown in Fig. 1(a) and (b). Both sets of computer models have the dimensions of 69 nm \times 69 nm \times 1.3 μ m, with each interface containing 114 \times 114 PbSe unit cells and 108 \times 108 PbTe unit cells. The dimensions of the interfaces are set according to the concept of coincidence site lattice on the misfit interface [54], with the normal strains along the x and y directions in both PbSe (under compressive strain) and PbTe layers (under tensile strain) being smaller than 3 \times 10⁻⁴. The interface regions are atomically resolved. The thicknesses of the atomic regions along the z direction are 25.4 nm and 27.4 nm \sim 33.8 nm for the one and two-interface

models, respectively. Coarse-scale finite elements (FEs) are used to discretize the remainder of the domain of the computational models, with the FE mesh size changing gradually from that in which each element contains 162 cubic unit cells to that containing 2888 cubic unit cells per element away from the interfaces. The elements have a square prism shape with {100} faces. The size of the atomic region assures that the stresses at the numerical interface between the atomic region and coarse FE region converge to that in the region away from the heterointerface, indicating that the use of FEs has no artificial effect on the simulation results. The absolute value of the shear stresses at the numerical interface is smaller than 3 \times 10⁻⁴ GPa, close to zero in the region away from the interface. The normal stresses are also close to that in the region away from the interface with difference smaller than 2%. The one-interface CAC model contains 3.9 million atoms and 15,480 elements. The two-interface model contains 6 million atoms and 15,480 elements. If resolved to fully atomistic models, each model would contain \sim 0.2 billion atoms. According to CAC finite element algorithm [55], the CAC models in this work reduce the degrees of freedom of an atomically resolved model by 97% and mathematical operations by 96.8%.

For the interaction between atoms in the heterostructures, we employ the empirical interatomic potential previously reported for PbTe/PbSe systems [24]. The potential was built on the transferrable potential for CdTe-CdSe-PbSe-PbS [23,56,57]. It is composed of a long-range Coulombic potential and a short-range Buckingham potential and is fitted to density functional theory (DFT) calculations and experimental measurements of several physical properties. The potential has been tested to reproduce the lattice parameters of bulk and alloy, the elastic constants, different phases, and the surface energies of PbTe and PbSe. The PbTe-PbSe potential has also been tested for CAC simulations in reproducing the misfit dislocation network [24], as well as the dislocation density as a function of the epilayer thickness [24], in good agreement with experimental observations [21,22,58]. The phonon dispersion relations for PbTe and PbSe calculated based on the interatomic potential using MD, CAC with the finest mesh size, and CAC with a coarse finite element mesh are presented in the Appendix, respectively. A comparison with first principles calculations is also included. The dispersion relations of acoustic phonons for both PbTe and PbSe single crystals calculated based on the potential are shown to agree reasonably well with first principles calculations [59]. However, the potential fails to reproduce the first principles results for optical phonons. It appears to be a common problem for existing classical force fields to reproduce the phonon dispersions of optical phonons in lead chalcogenides [60-62].

2.2. Misfit dislocation networks

The equilibrium structures of the PbTe/PbSe systems are obtained through simulations that mimic the direct wafer bonding process. It has been reported that heterostructures fabricated through direct bonding have only misfit dislocations at the interfaces and no threading dislocations in the epilayers [63]; the latter have been ubiquitously observed in strained heterostructures grown heteroepitaxially. In this work, the simulation of the direct wafer bonding process consists of three steps. In step 1, two single crystals are put into contact through pressure applied on the surfaces of PbTe and PbSe single crystals for 0.1 ns. In step 2, the bonded heterostructure is annealed through high-temperature simulations at 600 K for 0.2 ns, which is followed by a series of simulations with successively lowered temperatures from 600 K to 1 K and pressure lowered to 0 atm. The obtained heterostructure is further energy minimized in step 3. Periodic boundary conditions (PBCs) are applied along the lateral (i.e., x and y) directions. Pressure is applied on the surfaces along the cross-interface (i.e., z) di-

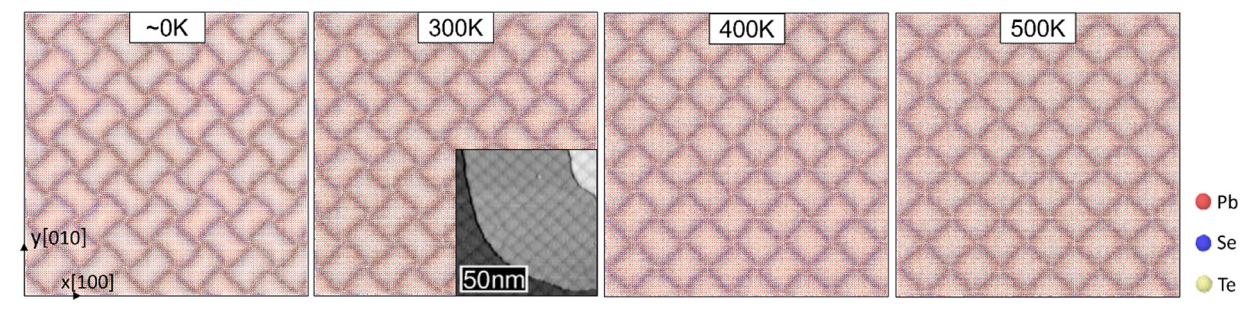


Fig. 2. The atomic structure of the PbTe/PbSe (001) semi-coherent interface at different temperatures. The interface area is $69 \text{ nm} \times 69 \text{ nm}$. The inset is a scanning tunneling microscopy image of the PbTe/PbSe (001) semi-coherent interface at 300 K from experiments (adapted from the figure in ref. [21]).

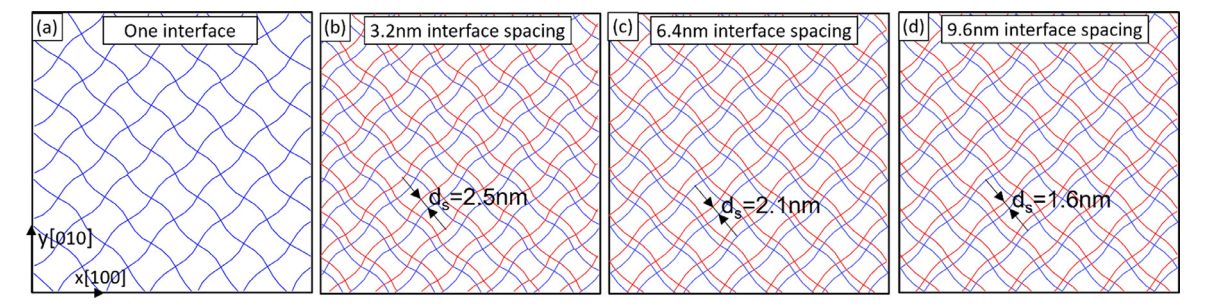


Fig. 3. (a)The DXA line-based representation of the misfit dislocation network within one PbTe/PbSe (001) interface. The DXA line-based representation of misfit dislocation networks within the two PbTe/PbSe (001) interfaces with interface spacings being (b) 3.2 nm, (c) 6.4 nm, and (d) 9.6 nm. The misfit dislocation network in the first interface is colored in blue and that in the second interface is colored in red. d_s indicates the shift distance between the misfit dislocation networks within the two interfaces along the [110] and [$\bar{1}$ 10] directions. The interface area is 69 nm \times 69 nm for each model. (For interpretation of the references to color in this figure legend, the reader is referred to the web version of this article.)

rection. The same procedure is used for computer models with one interface as well as those with two interfaces. To ensure that the equilibrium structures have the minimum potential energy, each heterostructure is obtained through simulations of 60 different relative positions between the PbTe layer and PbSe layer in the directions that are parallel to the interface. The simulations to find the equilibrium defect structures are most computationally intensive in this work.

The atomic structures of one PbTe/PbSe (001) semi-coherent interface at ~0 K is shown in Fig. 2. The dark lines indicate the misfit dislocations. It is seen from Fig. 2 that the misfit dislocation network is square-like, consisting of mixed a(100) and a/2(110)edge dislocations. At or below 300 K, about 90% misfit dislocations are a/2(110) dislocations, while \sim 10% misfit dislocations are a(100) dislocations. The $a\langle 100 \rangle$ dislocations are preferred near the dislocation junctions (the intersections of misfit dislocations) due to their lower core energy. The mixed-type dislocations make the network look slightly curved. At higher temperatures (≥400 K), the dislocation network becomes straight and only consists of a(110) dislocations, as shown in Fig. 2, which converges to the experimental observations of the PbTe/PbSe (001) misfit dislocation network at room temperature [21]. The average spacing of the dislocation network is 8.6 nm, in good agreement with the experimental result of 8.8 nm.

The obtained misfit dislocations in the equilibrated PbTe/PbSe structures are analyzed using the dislocation extraction algorithm (DXA) [64]. The line-based representations of the misfit dislocation networks are plotted in Fig. 3(a) for the one-interface model and in Fig. 3(b-d) for the two-interface models with interface spacings of 3.2 nm, 6.4 nm, and 9.6 nm, respectively. As can be seen from Fig. 3 (b-d), the dislocation networks in the two-interface models remain square-like with the average spacing of 8.6 nm. It is noticed that the two misfit dislocation networks in the structures with two interfaces do not overlap when viewed in the direction perpendicular to the interfaces. Rather, there are shift distances, d_s , between the two misfit dislocation networks, which are 2.5 nm, 2.1 nm, and

1.6 nm, respectively, along the [110] and $[\bar{1}10]$ directions for the three specimens shown in Fig. 3 (b-d).

In Fig. 4 we present side views of the atomic stress components σ_{xx} , τ_{xy} , and τ_{xz} near the misfit dislocations, in which the atomic core structure of the misfit dislocations can be clearly observed. The stress distribution, especially the shear stress, is seen to be greatly influenced by the neighboring interface and the interface spacing. This effect gradually diminishes as the interface spacing increases

3. Phonon-dislocation interaction in PbTe/PbSe (001) heterostructures

3.1. Comparing CAC and MD

The phonon wave packet (PWP) technique [65] is employed in the simulation of the scattering of phonon pulses by misfit dislocations. A phonon is a quantized mode of vibration in a crystal lattice and so each phonon mode is specified by a wave vector \mathbf{k} and an eigenvector \mathbf{e} . A wave packet is a linear combination of phonon modes centered at a specific wave vector. The advantage of using PWP is that it can quantitatively measure the mode dependence of the phonon-dislocation interaction and provide a visualization of the process of phonon-dislocation interaction. The phonon wave packet at position $\mathbf{r_0}$ with a central wave vector \mathbf{k} can be constructed by applying the displacement field \mathbf{u} according to

$$\mathbf{u}(r) = U\mathbf{e} \exp\left[i\mathbf{k}(r - r_0)\right] \times \exp\left[-\frac{(r - r_0)^2}{\eta^2}\right]$$
 (2)

where U is the amplitude, \mathbf{e} is the eigenvector, \mathbf{r} is the position of the atom or the FE nodes, and η is the spatial extent.

In this study, the wave packets are constructed in the PbSe region of the computer model and allowed to propagate along the z direction towards the PbTe/PbSe interface. For wavevectors along the z direction (i.e., [001] direction) there is one longitudinal acoustic (LA) phonon branch, two transverse acoustic (TA) phonon

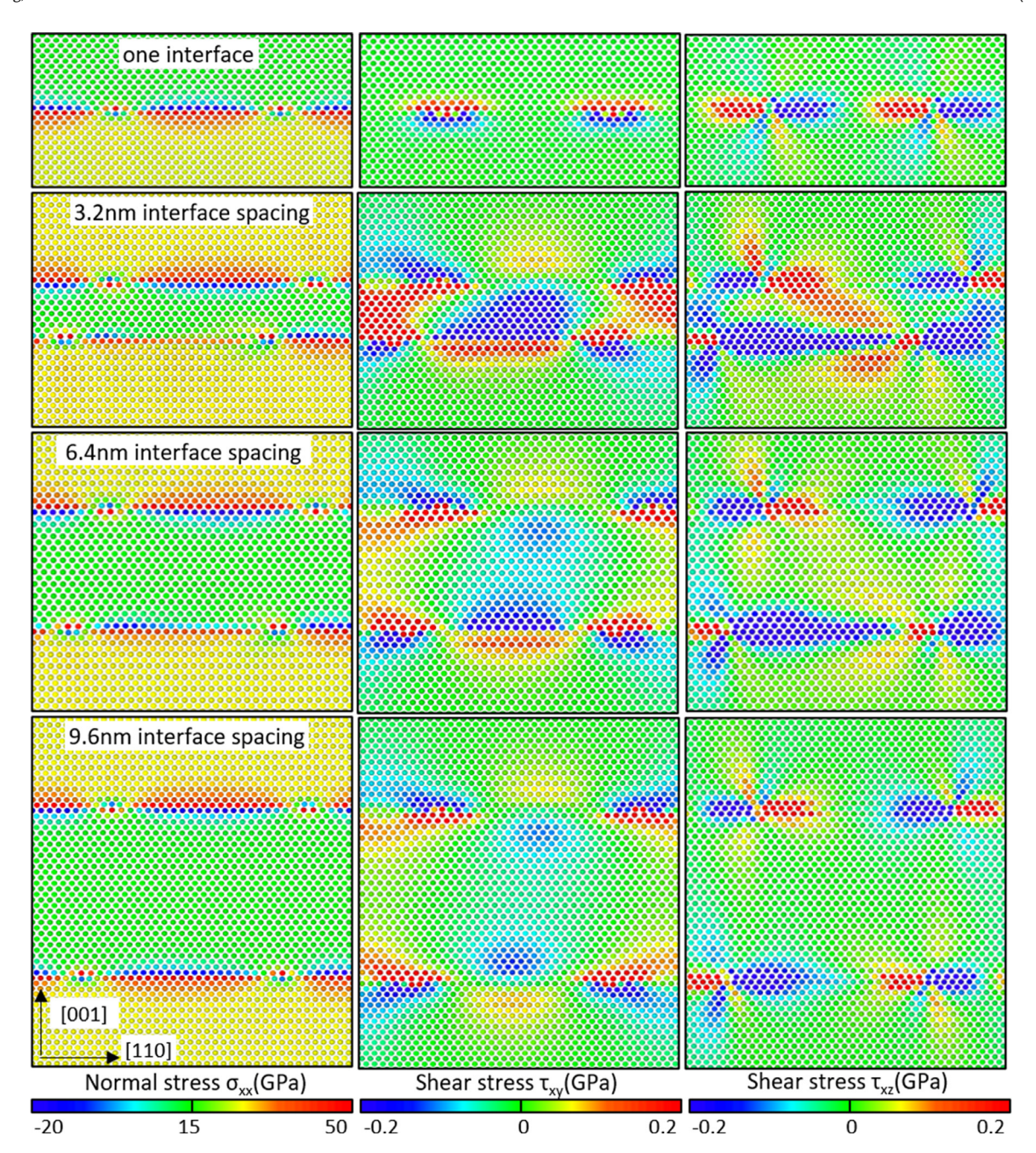


Fig. 4. Stress σ_{xx} (1st column), τ_{xy} (2nd column), and τ_{xz} (3rd column) near the misfit dislocations in the heterostructures with one interface (1st row), and two interfaces with interface spacings of 3.2 nm (2nd row), 6.4 nm (3rd row), and 9.6 nm (4th row). For visualization purpose, only Pb atoms are shown.

branches, one longitudinal optical (LO) phonon branch, and two transverse optical (TO) phonon branches. LA and LO phonon modes have the polarization vectors along the [001] direction. The two TA branches and two TO branches are degenerate due to the cubic crystal symmetry. The polarization vectors of the TA and TO phonon modes can be in any pair of orthogonal directions perpendicular to [001]. In this study, the LA and LO phonon pulses are constructed based on the LA and LO phonon modes with polarization vectors along the [001] direction; the TA and TO phonon pulses are constructed based on the TA and TO phonon modes with polarization vectors along the [110] direction. It is worth noting that we have also simulated phonon pulses based on the TA and TO phonon modes with polarization along the [100] and [010] directions, respectively. The simulation results are similar to that of the [110] direction.

To test the accuracy of the CAC models that contain coarse-scale FEs with respect to MD, we have built a fully resolved atomistic model with dimensions of $69 \text{ nm} \times 69 \text{ nm} \times 100 \text{ nm}$ that contains 16.2 million atoms. We then simulate the propagation of a set of TA phonon pulses with different wavelengths using both the atomically resolved and the coarse-grained models. Simulation results show that the two computer models converge as the phonon wavelength increases. Fig. 5 compares the displacements during the propagation of the phonon pulse that has central wavelength of 8 nm in the two models. As can be seen, the displacements obtained in the two simulations agree very well, despite their different resolutions. After the scattering process, the incident phonon pulse has transited into a reflected phonon pulse in the PbSe layer and a transmitted phonon pulse in the PbTe layer. By measuring the kinetic energy of the transmitted

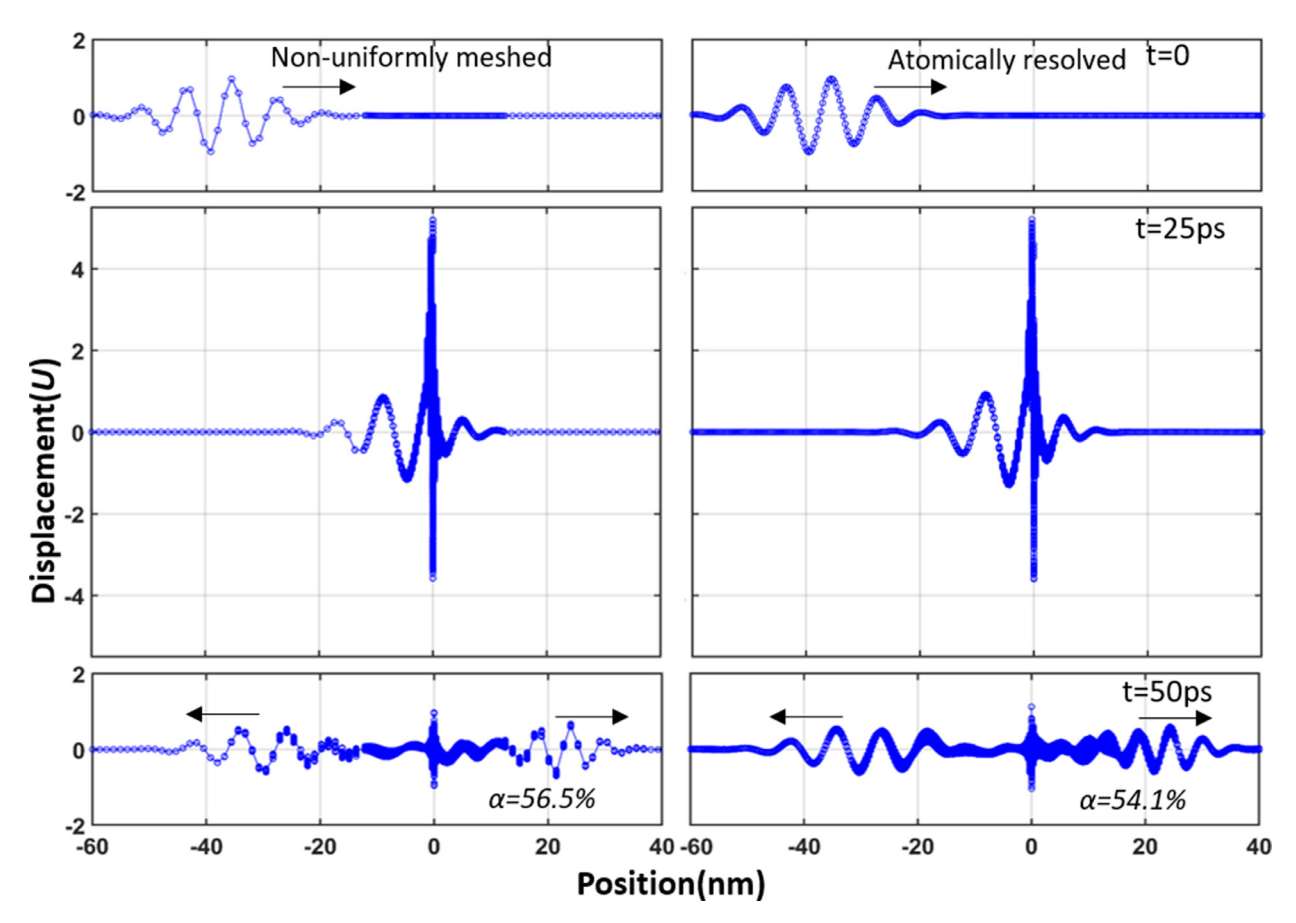


Fig. 5. Time sequences of the displacement field of the PbTe/PbSe (001) heterostructure during the propagation of a TA phonon pulse with wavelength of 8 nm, simulated using CAC with coarsely meshed finite elements (left) and MD with atoms (right). The unit of the displacement, *U*, denotes the amplitude of the incident phonon wave packet, which is 0.001 Å.

phonon pulse $(E_{\rm T})$ and the kinetic energy of the initial phonon pulse (E), the energy transmission coefficient can be calculated by $\alpha=E_{\rm T}/E$. The calculated energy transmission coefficients of the phonon pulses across the interface in the two models are 56.5% and 54.1%, respectively. The maximum vibrational amplitude of the misfit dislocations in response to the phonon pulse is 5.2 U in both models, where U=0.001 Å is the amplitude of the incident wave.

These comparisons demonstrate that CAC can reproduce phonon-dislocation interaction with the accuracy of MD for nonequilibrium processes involving phonons with wavelength longer than 8 nm for the PbTe/PbSe (001) heterostructures studied in this work. By allowing multiscale resolutions, CAC can significantly reduce the degrees of freedom, and consequently increase the length scale of the studied specimen, while at the same time accurately reproduce the atomic-level structures of dislocation cores. The unified governing equation for both the fully atomic and the coarse-scale FE regions guarantees that the propagation of long-wavelength phonons across the numerical interfaces between different resolutions has no unphysical wave reflections [66,67]. CAC thus has the unique ability to address the length scale challenge in studying phonon scattering by multiple dislocations without any assumption of empirical rules. It is worth noting that CAC can simulate optical phonons, as it describes the internal vibrations of atoms within each unit cell. The limitation of CAC is that it cannot directly simulate phonons with wavelengths smaller than the FE mesh size. Since CAC has been demonstrated to have the accuracy of MD in simulating phonons with wavelength equal or larger than 8 nm, as shown in Fig. 5, in this work, phonons of wavelength ranging from 8 nm to 121 nm are simulated using the nonuniformly meshed models (69 nm \times 69 nm \times 1.3 μ m), while those with phonons whose wavelengths are smaller than 8 nm are simulated using the atomically resolved smaller models (69 nm \times 69 nm \times 0.1 μ m).

3.2. Phonon scattering by misfit dislocations and phonon energy transmission across the misfit interface

The obtained PbTe/PbSe (001) heterostructure with a single interface is simulated under the excitation of ultrashort acoustic phonon pulses, with the central wavelengths of the pulses ranging from 0.7 nm to 121 nm. To quantify the effect of misfit dislocations on phonon energy transmission, we have also built a model that has the same length as the CAC model, i.e., 1.3 μ m, but has a coherent interface formed by 4 × 4 PbTe unit cells and 4 × 4 PbSe unit cells with PBCs applied in the lateral directions of the model. While such an ideal structure does not physically exist, simulation results of the model can be used to quantify the role of misfit dislocations, as the small cross-sectional area confined by the imposed PBCs prevents misfit dislocations from nucleating, resulting in a heterostructure with a dislocation-free, i.e., coherent, interface.

In Fig. 6(a) and (b), we present the mode-wise energy transmission coefficients of TA and LA phonons, respectively, across the misfit interface, as well as their comparisons with that across the coherent interface. To quantify the dislocation reaction to the phonon pulses, in Fig. 6(c) and (d), we plot the maximum vibra-

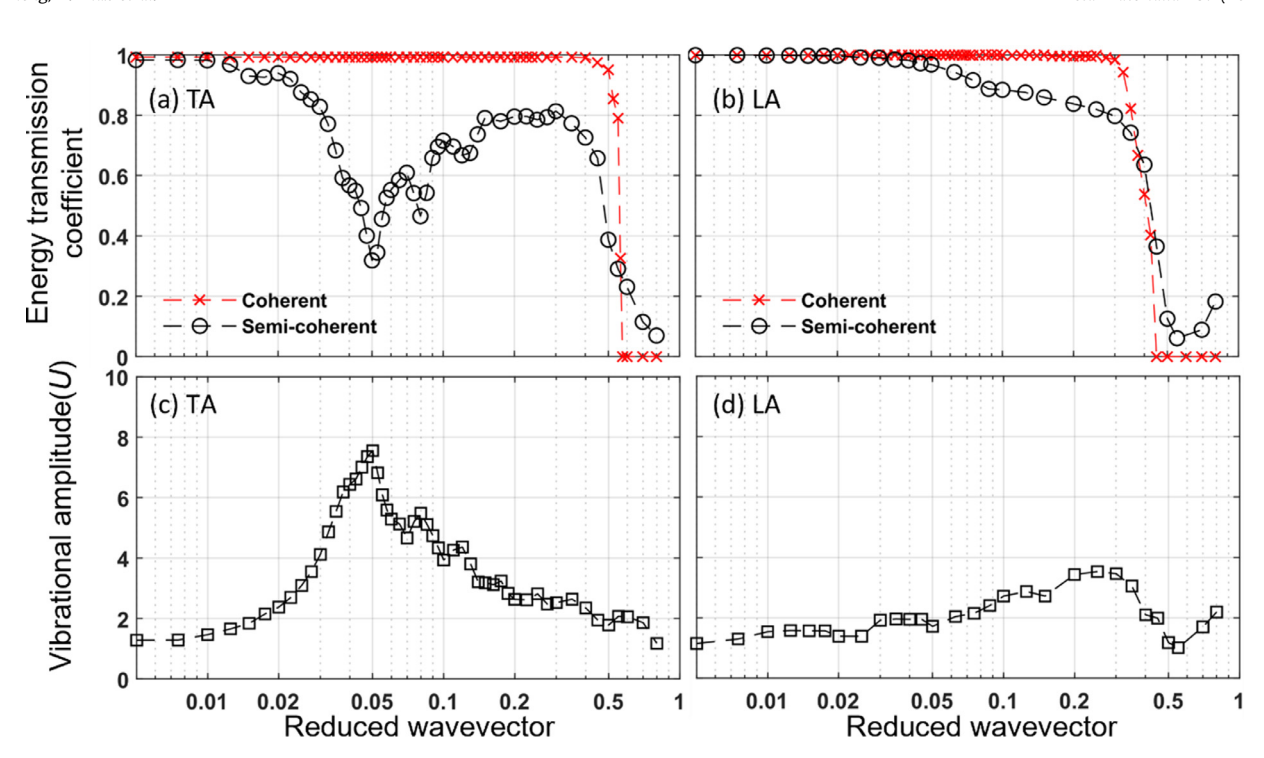


Fig. 6. The mode-wise energy transmission coefficients of (a) TA and (b) LA phonons across the semi-coherent and coherent single PbTe/PbSe (001) interfaces. The vibrational amplitude of the misfit dislocations in the interaction with the (c) TA and (d) LA phonon pulses with different wavevectors. The unit *U* denotes the amplitude of the phonon pulse, which is equal to 0.001 Å.

tional amplitudes of the misfit dislocation network, in terms of the amplitude of the incident phonon pulse, as a function of the central wavevector of the phonon pulses. To provide a visualization of phonon scattering by the interface, Fig. 7 presents the time sequences of the displacement responses to a TA and a LA phonon pulse, respectively. Major observations from Figs. 6 and 7 may be summarized as follows.

- (1) The energy transmission coefficients of the TA and LA phonon modes across the *coherent* interface are very high, except the high-frequency large-wavevector phonons; the latter is a result of the mismatch between the phonon dispersion relations of PbTe and PbSe, since this mismatch increases with the wavevector. By contrast, the energy transmission coefficients across the semi-coherent interface are much lower, as shown in Fig. 6(a) and (b). This difference reflects the effect of the misfit dislocations on phonon transport across the interfaces.
- (2) There is also a large difference in energy transmission between TA and LA phonons, as shown in Fig. 6(a) and (b), suggesting two different phonon-dislocation scattering mechanisms, which are supported by the discontinuous and continuous displacement fields at the locations of the misfit dislocations under the TA and LA phonons, respectively, as shown in Fig. 7.
- (3) Consistent with the relatively larger energy transmission of the LA phonons, the dislocation reaction to the LA phonons is much weaker, with the vibrational amplitude of the dislocations in response to the LA phonons being 2 to 3 times smaller than that to the TA phonons, as shown in Fig. 6(c) and (d).
- (4) Unlike that of LA phonons, the energy transmission of TA phonons exhibits a series of local minima, e.g., at frequencies of 0.115 THz, 0.183 THz, 0.273 THz, and 0.395 THz (reduced wavevectors of 0.05, 0.08, 0.12, and 0.175), with the TA phonon mode with frequency of 0.115 THz (wavelength 12.1 nm) having the lowest energy transmission coefficient of 31.9%, as shown in Fig. 6(a).
- (5) Corresponding to the local minima of energy transmission coefficients, the dislocation vibrational amplitudes exhibit local maxima at the same frequencies, as shown in Fig. 6(c). This implies that at certain frequencies, local modes of the misfit dislocations are excited by the TA phonon pulses, leading to resonant interaction between phonons and the misfit dislocations. Specifically, the largest dislocation vibration amplitude occurs when the energy transmission coefficient is the lowest for the phonon pulse whose central wavelength is 12.1 nm and frequency 0.115 THz, as shown in Fig. 6(a) and (c), at which the misfit dislocations experience the highest vibration amplitude of 7.6 U, where U = 0.001 Å is the amplitude of the phonon pulse in all of the figures in this work. Fig. 7 confirms that the majority of this phonon pulse is reflected back by the interface, resulting in the lowest energy transmission of 31.9%; there is clearly a co-existence of spectral and diffusive phonon scattering by the misfit dislocations with the spectral scattering being dominant. In contrast, the LA phonon pulse is only weakly scattered, with a high energy transmission coefficient of 96.8%. It is worth mentioning that we have also simulated phonon pulses with U = 0.002 Åand 0.003 Å, respectively, and obtained similar results. This indicates that when U is small, the energy transmission coefficients and the dislocation vibrational amplitude (in the unit of U) do not depend on the amplitude of the phonon wave packets.
- (6) For the TA phonon pulse shown in Fig. 7, the displacement fields are discontinuous at the locations of the misfit dislocations that have the Burgers vector along [110] but continuous at those with the Burgers vector along [110]. However, the displacement field is continuous at the locations of all the dislocations for the LA phonon pulse. The displacement discontinuity across misfit dislocations indicates the excitation of local modes of dislocations by phonons whose polarization vectors are parallel to the Burgers vectors of dislocations.

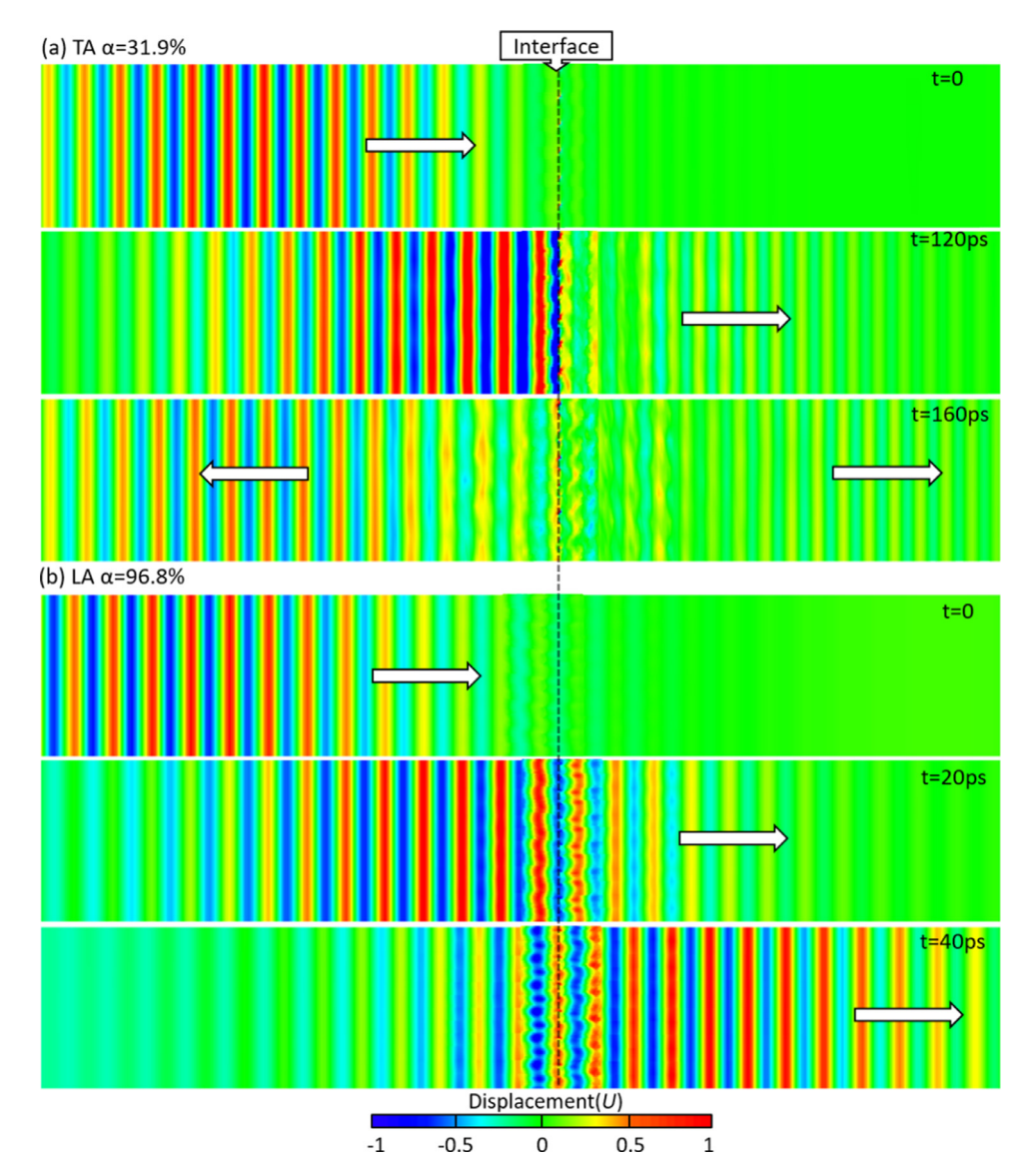


Fig. 7. Time sequences of zoomed-in displacement contours during the propagation of (a) the TA and (b) the LA phonon pulses with wavelength of 12.1 nm in the PbTe/PbSe (001) heterostructure that contains one interface, showing phonon scattering by the misfit dislocations. The interface is marked by the dashed line. The arrows show the travelling directions of the phonon pulses. The energy transmission coefficients of the TA and LA phonon pulses are 31.9% and 96.8%, respectively.

Although the interatomic potential does not reproduce the phonon dispersions of optical phonons for PbTe and PbSe with DFT accuracy, it still reproduces the essential features of the optical phonons: the high-frequency out-of-phase movements of the atoms within the unit cell. Since the phonon dispersions of optical phonons in PbTe and PbSe obtained from the interatomic potential are completely mismatched, which leads to zero energy transmission coefficients across the interface, we focus on investigating the nature of the scattering of optical phonons by misfit dislocations. In Fig. 8 we present the time sequences of the displacement response of the PbTe/PbSe heterostructure to a TO phonon pulse with wavelength 6.1 nm and frequency 4.24 THz. As can be seen, the scattering of optical phonons by misfit dislocations is dominantly diffusive, as the scattered TO phonon pulse completely loses the coherency. Meanwhile, the vibrational amplitudes of the atoms near the misfit dislocations are negligibly small (<0.1 U) during the interaction. This means no local vibrational modes of the misfit dislocations are excited by the optical phonons. Similar phenomena are observed for other optical modes.

With the energy transmission coefficients for the phonon modes spanning the entire Brillouin zone, the thermal boundary resistance (TBR) of the PbTe/PbSe (001) misfit interface can be quantified based on the Landauer formalism. The Landauer formula relates the electrical resistance of a quantum conductor to the scattering properties of the conductor [68]. The formalism has been widely used to quantify the thermal conductance in terms of the energy transmission of phonon modes, assuming that each material at the interface has equilibrium phonon distributions [69]. This assumption breaks down when the average phonon transmission is close to unity. Landry and McGaughey modified the formula such that it is valid for nonequilibrium phonon distributions. In this work, the expression for TBR developed by Landry and Mc-Gaughey based on the Landauer formalism is employed [70]. The phonon lifetimes in the expression are calculated using ALAMODE [71]. The thermal resistance of the PbTe/PbSe (001) misfit interface at 1 K is calculated to be 9.1×10^{-8} Km²/W. This value will be compared with the thermal resistance of the interface with pinned misfit dislocations in the next section. It is worth noting that at

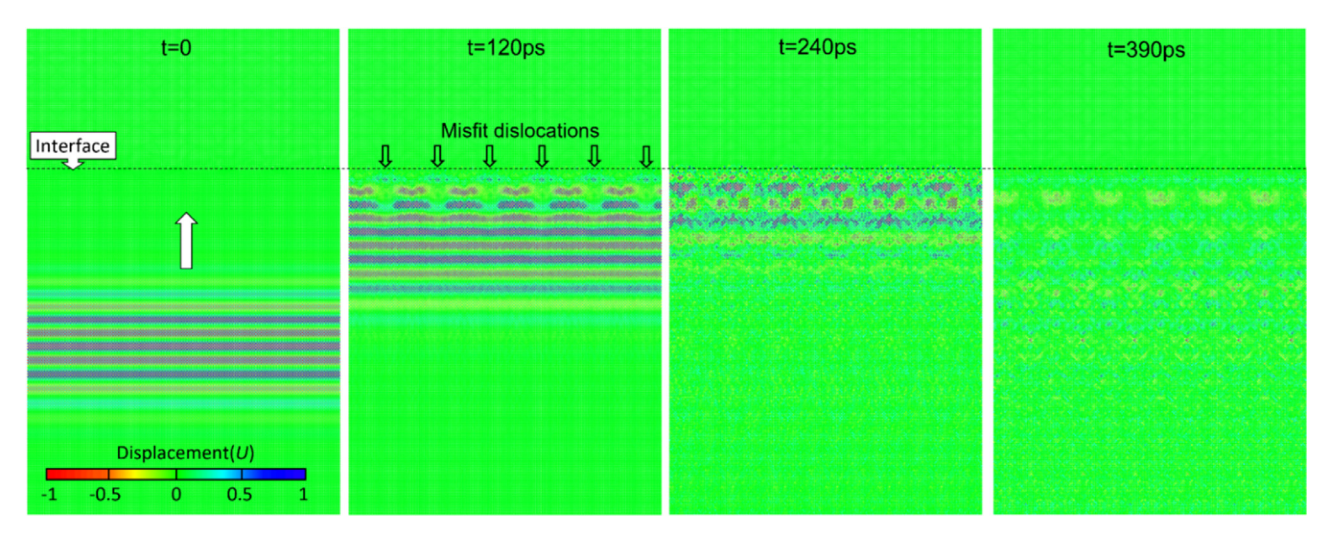


Fig. 8. Time sequences of zoomed-in displacement field during the propagation of the TO phonon pulse with wavelength of 6.1 nm and frequency of 4.24 THz in the PbTe/PbSe (001) heterostructure that contains one interface. The interface is marked by the dashed line. The white arrow indicates the traveling directions of the phonon pulses.

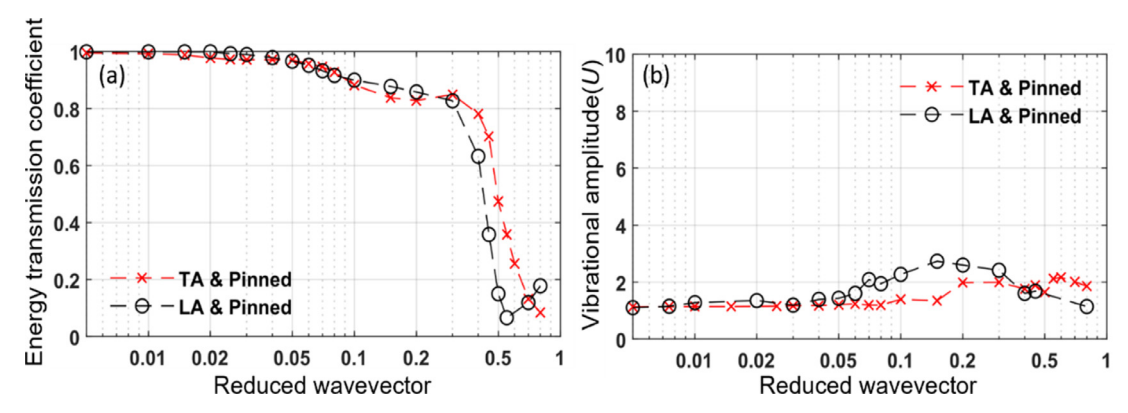


Fig. 9. (a) The mode-wise energy transmission coefficients of TA and LA phonons across the PbTe/PbSe (001) interface containing pinned misfit dislocations; (b) The vibrational amplitudes of the pinned misfit dislocations during the phonon-dislocation interaction as a function of wavevector.

low temperatures the contribution of optical phonon scattering to the interfacial thermal resistance is negligible.

3.3. Local vibrational modes of misfit dislocations and the collective motion of the dislocation networks

To quantify the role of the local vibrational modes of misfit dislocations, point defects are induced into the PbTe/PbSe (001) interface to pin the movement of the misfit dislocations. This is achieved through removing atoms near the misfit dislocations (for each misfit dislocation segment, 4 atoms are removed). The TA and LA phonon energy transmission coefficients are presented in Fig. 9(a). The vibrational amplitudes of the dislocations under the excitation of TA and LA phonons are plotted in Fig. 9(b). Comparing Fig. 9 with Fig. 6, we see that the vibrations of the misfit dislocations under the LA phonons are only slightly weakened by the point defects, with the energy transmission coefficients being almost unaffected. This indicates that the scattering of LA phonons at the interface is caused by the strain field of the dislocations rather than by the vibrations of dislocations. In contrast, the vibrations of misfit dislocations under TA phonons are significantly weakened by the point defects, as the energy transmission coefficient of the TA phonon pulse with frequency of 0.115 THz increases from 31.9% (before pinned) to 97% (after pinned), which is very close to that for the LA phonons across the same misfit interface. These results demonstrate that the interaction between TA phonons and misfit dislocations is dominated by the dynamic mechanism, i.e., the excitation of local vibrational modes of misfit dislocations, and the resonant interaction is responsible for the low energy transmission and strong dislocation vibrations. By contrast, the static mechanism is responsible for the weak interactions between LA phonons and misfit dislocations, as it does not excite local dislocation vibrational modes. The thermal resistance of the interface with pinned misfit dislocations at 1 K is calculated to be $1.4 \times 10^{-8} \ \mathrm{Km^2/W}$, which is about 1/6 that of the interface with unpinned misfit dislocations. This large difference in TBR indicates again that the resonant interactions play a significant role in the thermal resistance of PbTe/PbSe (001) misfit interface.

To visualize the vibrational modes of dislocations, Fig. 10(a) and (b) present snapshots of the displacements of atoms at the PbTe/PbSe (001) interface in response to a TA phonon pulse and a LA phonon pulse, respectively. The central frequency of the TA phonon pulse is 0.115 THz and that of the LA phonon pulse is 1.53 THz. These two particular TA and LA phonon pulses were found to excite the strongest vibrations of dislocations, respectively, among all the TA and LA phonon pulses we have simulated. It is seen from Fig. 10 that, for both TA and LA phonon pulses, atoms near the dislocations experience higher amplitude of collective vibrations than the rest of the atoms. However, the reactions of misfit dislocations to TA and LA phonon pulses are different in vibration amplitude and displacement pattern. Under the TA phonon pulse, each dislocation line segment deforms approximately in the shape of a bow or a half-sine wave, with the dislocation junctions in the dislocation network acting as pinning

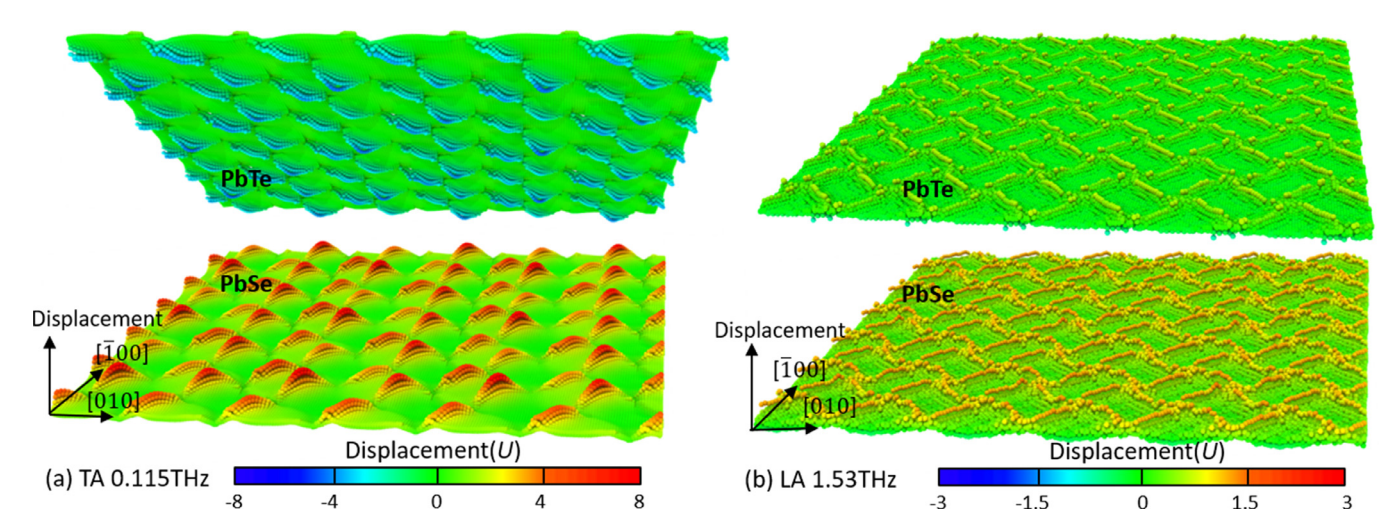


Fig. 10. Snapshots of the displacements of the PbSe atoms and the PbTe atoms at the interface during the propagation of (a) a TA phonon pulse with frequency of 0.115 THz and (b) a LA phonon pulse with frequency of 1.53 THz.

points of the dislocations, as shown in Fig. 10(a). The atoms near the dislocation segments also move concomitantly with dislocations, leading to the deformation shape of a 3D surface. In addition, the PbSe and PbTe atoms near the dislocations at the two sides of the interface vibrate in opposite directions. By tracking the time histories of the displacements of these atoms, we find that these atoms are subjected to out-of-phase vibration under all the TA phonon pulses. However, not all the dislocations in the network exhibit local out-of-phase vibration. Only the misfit dislocations with Burgers vectors in the [110] direction vibrate with this local mode, while the misfit dislocations that lie along the [110] direction with Burgers vectors in the [110] direction do not. Note that the polarization vectors of the incident TA phonons are along the [110] direction. This indicates that the local dislocation vibrational mode can only be activated by phonons that can provide shear-stress components along the Burgers vectors of the dislocations. When the polarization vectors of the incident TA phonons are along the [100] direction, the local vibrational modes of all the misfit dislocations (with the Burgers vectors along the [110] and [110]directions) are activated, as the phonons can provide the shear-stress component along the Burgers vectors of all the dislocations. It is the out-of-phase vibrations that lead to the discontinuous displacement fields at the locations of dislocations shown in Fig. 7(a).

In contrast to the TA phonon pulses, the vibrations of the misfit dislocations in response to LA phonon pulses do not depend on the relationship between the polarization vectors of the phonons and the Burgers vectors of dislocations. This is because the polarization vectors of LA phonons are along the z (longitudinal) direction, which is perpendicular to the Burgers vectors of all the misfit dislocations. As a result, all the misfit dislocations at the interface vibrate, together with the rest of the atoms near the interface, with a larger amplitude but nearly uniform vibrational amplitude, as shown in Fig. 10(b). No out-of-phase vibrations of dislocations are observed for any LA phonon pulse. Consequently, the displacement field is continuous with all LA phonon pulses. Thus, although the misfit dislocation networks vibrate under the influence of either TA or LA phonon pulses, only the TA phonons excite the local modes of the misfit dislocations. The widely speculated and discussed fluttering of dislocations [6] described in the dynamic theories is thus the out-of-phase vibrations of the atoms on the two sides of the slip plane, and such vibrational mode can only be excited by the TA phonons. Contrary to what Roth and Anderson [6] believed, LA phonons do not excite the out-of-phase dislocation vibrations and hence are only weakly scattered by misfit dislocations in this study. This also points to the likelihood of TA phonon modes being responsible for any restructuring of the interfaces with misfit dislocations.

In Fig. 11, we present six snapshots of the zoomed-in displacements of the PbSe atoms at the interface under different TA phonon pulses. It is seen that for the phonon pulses with central frequencies of 0.029 THz and 0.115 THz, the dislocation segments vibrate in a similar pattern. By examining the dislocation reactions to the TA phonon pulses, we find that for TA phonon pulses with frequencies below 0.115 THz, the dislocation segments all vibrate approximately with the shape of a half-sine wave. This means that the same local dislocation vibrational mode is excited during the excitations of all these phonon pulses. As the frequency increases, the vibrational modes become more and more complex, having the shape of two, three, or more, half-sine waves. They are higherorder vibrational modes. We thus conclude that the lowest-order mode is the one with the vibrational frequency of 0.115 THz, which has the strongest resonant interaction with the TA phonon pulse of the same frequency.

In addition, a collective motion of the dislocation segments, i.e., the misfit dislocation network, can be observed for all the TA phonon pulses. In Fig. 12, we present snapshots of the time history of the reaction of the misfit dislocations to the TA phonon pulse with central frequency of 0.115 THz. It is seen that the dislocation segments, which are pinned at the dislocation junctions, do not vibrate uniformly or randomly. Rather, there is a clear pattern of the motion of the entire misfit dislocation network, in which the dislocations vibrate cooperatively. This is a demonstration of the collective motion of the dislocation segments at the misfit interface.

3.4. Phonon-dislocation interaction in heterostructures with two interfaces

If there is the collective motion of misfit dislocations due to the long-range interaction between dislocations, then the presence of an additional misfit interface should influence the vibrational motion of the dislocation network that is localized at each interface. To confirm this and to characterize its nature, CAC simulations of PbTe/PbSe (001) heterostructures containing two interfaces with interface spacings of 3.2 nm, 6.4 nm, and 9.6 nm, respectively, are performed for ultrafast acoustic phonon pulses with the central wavelength ranging from 0.7 nm to 121 nm. The nonequilibrium processes of scattering of the phonon pulses by the misfit

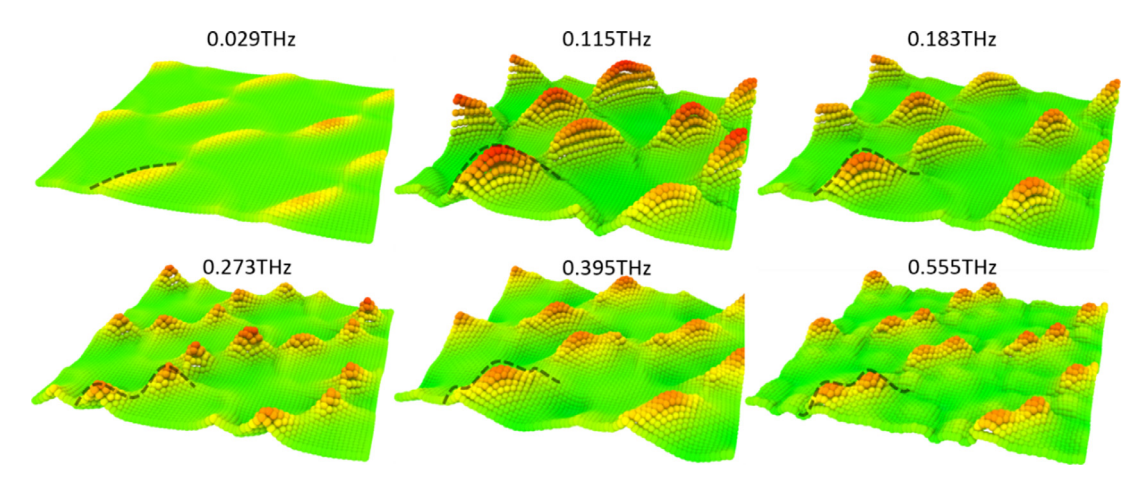


Fig. 11. Snapshots of the displacements of the PbSe atoms at the interface under TA phonon pulses with the varying frequencies, among which the frequencies of 0.115 THz, 0.183 THz, 0.273 THz, 0.395 THz, and 0.555 THz correspond to the local maximum values of the dislocation vibrational amplitudes in Fig. 6(c); only a small region of the interface is shown. The dashed lines are plotted to indicate the vibrational mode shapes of the dislocation segments.

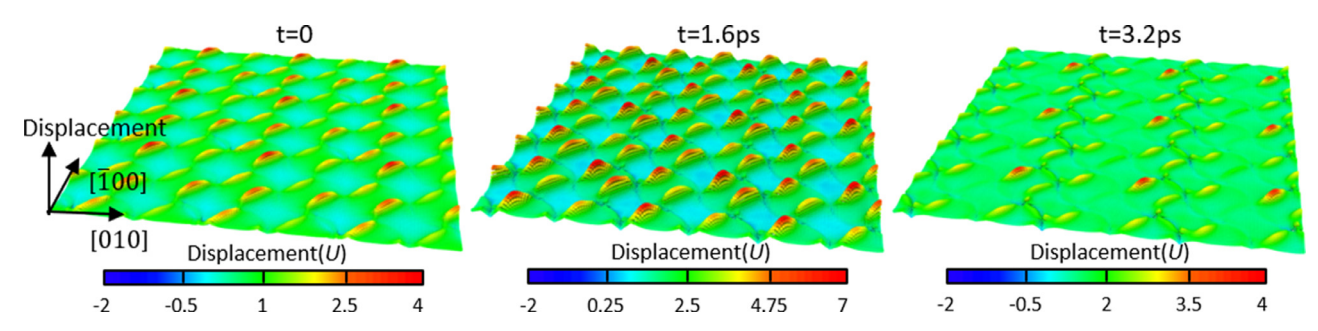


Fig. 12. Time sequence of snapshots of the displacements of the PbSe atoms at the interface under the TA phonon pulse with frequency of 0.115 THz.

dislocations are again visualized, and the energy transmission coefficients are determined. For comparison purposes, we have also built a set of models that have the same length as the CAC models, i.e., 1.3 μm , but contain two coherent interfaces with interface spacings of 3.2 nm, 6.4 nm, and 9.6 nm, respectively, formed by 4 \times 4 PbTe unit cells and 4 \times 4 PbSe unit cells with periodic boundary conditions applied in the lateral directions of the model to quantify the effect of misfit dislocations on phonon-dislocation interaction.

In Fig. 13, we present the simulation results of mode-wise energy transmission coefficients of TA phonons across the two semicoherent interfaces as well as the vibrational amplitude of the misfit dislocations, compared with the heterostructures with one interface and two coherent interfaces, respectively. In Fig. 14, we present the snapshots of the displacements of the PbSe atoms at the two interfaces, respectively, in the heterostructures with different interface spacings.

Comparing the results of the heterostructures having two interfaces with that having one interface, we summarize the following similarities and differences in phonon-dislocation interaction between the two types of heterostructures.

- (1) The phonon-dislocation interaction is much stronger in the heterostructures with two interfaces than that with one interface. In particular, for the two-interface heterostructure with interface spacing of 6.4 nm, the largest dislocation vibration amplitude is 9.2 U, while that with one interface is 7.6 U; for the two-interface heterostructure with interface spacing of 9.6 nm, the lowest energy transmission coefficient is 3.9%, while that with one interface is 31.9%.
- (2) The wavevector or frequency with which the misfit dislocations have the strongest reaction has changed relative to the case of

- a single interface. As an example, for the two interfaces with 3.2 nm interface spacing, the frequencies of the phonon pulses for the largest dislocation vibrational amplitude and the lowest energy transmission are 0.092 THz and 0.098 THz, respectively, while that with one interface is 0.115 THz. This means the presence of an additional interface alters the atomic arrangements near the dislocations and infers a change in the local vibrational modes of the dislocation networks.
- (3) Both the energy transmission and maximum dislocation vibrational amplitude, as well as the frequencies for the strongest interaction, change with the interface spacing. For example, the central frequencies that lead to the strongest dislocation vibrations are 0.092 THz, 0.115 THz, and 0.126 THz for interface spacings of 3.2 nm, 6.4 nm, and 9.6 nm, respectively.
- (4) Similar to that with one interface, both the energy transmission coefficients and the dislocation vibrational amplitudes exhibit a series of local minima and local maxima, respectively. However, there are small but noticeable differences between the frequencies for the local minima of energy transmission coefficients and the local maxima for dislocation vibrational amplitudes. For example, for the heterostructure with 3.2 nm interface spacing, the central frequency of the phonon pulse that has the lowest energy transmission is 0.098 THz (reduced wavevector of 0.043), while that for the largest dislocation vibrational amplitude is 0.092 THz (reduced wavevector of 0.04).
- (5) For each of the three heterostructures that contain two interfaces, the lowest-order mode, i.e., the mode with lowest frequency, remains the one in which each dislocation segment vibrates in the shape of a half-sine wave and has the strongest resonant phonon-dislocation interaction, as shown in Fig. 14.
- (6) There is a local minimum for the energy transmission coefficients at a smaller wavevector before the lowest energy trans-

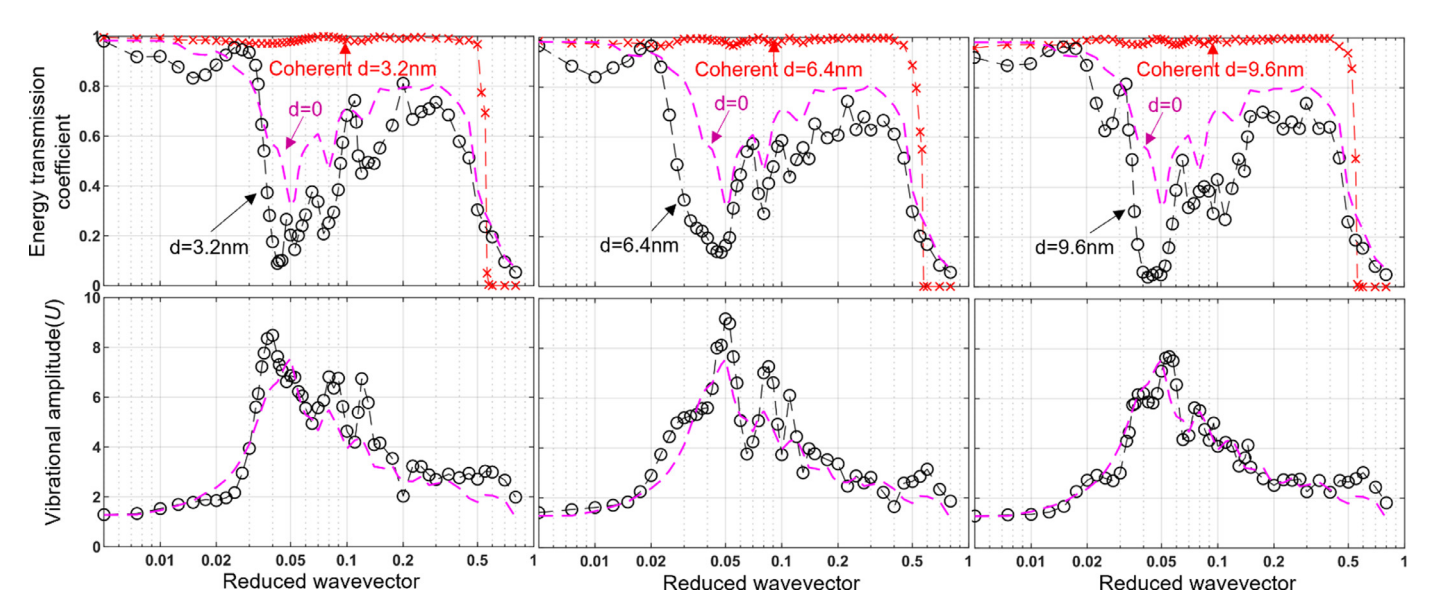


Fig. 13. Upper row: mode-wise energy transmission coefficients of TA phonons across two-interfaces; lower row: dislocation vibrational amplitude, with interface spacing d = 3.2 nm, 6.4 nm, and 9.6 nm, respectively. The mode-wise energy transmission coefficients and vibration amplitude of misfit dislocations in PbTe/PbSe (001) heterostructures with one interface (d = 0) and that with two coherent interfaces are included for comparison. The unit U denotes the amplitude of the phonon pulse, which is equal to 0.001 Å.

mission coefficient in each heterostructure. There is, however, no corresponding local maximum for dislocation vibration near that frequency. By checking the displacement contour with the phonon pulse of that frequency, we found that the dislocations still vibrate in the shape of a half sine wave. It is thus not a different local vibrational mode. The local minimum is thus probably caused by factors other than dislocations, such as wave interference due to the presence of two interfaces. This is likely also the reason why the lowest energy transmission and largest dislocation reaction do not occur at the same phonon pulse when there are two interfaces.

4. Summary and discussion

In this work, we have obtained the equilibrium structure of the misfit dislocation network at the PbTe/PbSe (001) interface through simulations that mimic the direct wafer bonding process. The misfit dislocation network is square-like, consisting of pure edge dislocations with average dislocation spacing of 8.6 nm, which compare reasonably well with experimental observations by Springholz and Wiesauer [21]. For the heterostructures with two interfaces having interface spacings of 3.2 nm, 6.4 nm, and 9.6 nm, the dislocation networks remain square-like and have the same average dislocation spacing of 8.6 nm. However, there are shifts of 2.5 nm, 2.1 nm, and 1.6 nm, respectively, in the dislocation positions between the two interfaces along the [110] and [110] directions.

Through visualizing the dynamic interaction between phonons and misfit dislocations, this work has illustrated and quantified two mechanisms for phonon-dislocation interaction: (1) phonon scattering by the strain field of dislocations, and (2) phonon scattering by dislocations that vibrate via the local modes of a dislocation network. The former is the "static mechanism" termed by Nabarro [2], which underlies the reactions of the misfit dislocations to LA, TO, and LO phonons in the PbTe/PbSe (001) heterostructures, while the latter is similar to the concept of fluttering dislocations [13], which are found in the reactions of misfit dislocations to TA phonons in this work. By comparing the energy transmission coefficients of the TA phonons across the unpinned misfit dislocation network with that across pinned misfit dislocation network, this work confirms the strong role of local vibrational modes

of dislocations in phonon transport. Also, by comparing the energy transmission coefficients of phonon pulses across the misfit dislocation interfaces with that across coherent (dislocation-free) interfaces, this work demonstrates the significant role of misfit dislocations in the thermal resistance of the PbTe/PbSe (001) heterostructures

We have also quantified the local vibrational modes of the dislocations. Local dislocation vibrational modes were first discussed by Ninomiya who related the resonant frequencies to the localized modes of a dislocation [72]. Simulations in this work demonstrate that there are a series of such resonant modes, which are manifested as local maxima of dislocation vibrational amplitude and out-of-phase vibrations of the atoms on the two sides of the slip plane, leading to a local minimum in the energy transmission coefficients in the heterostructure that contains one interface. Among the resonant modes, the lowest-frequency mode is one for which each dislocation segment vibrates with the shape of a halfsine wave and has the largest dislocation vibration amplitude; for higher-frequency modes, the vibrational shapes of dislocation segments are very complex, making it unlikely for a simple theoretical model to quantitatively predict material performance. In addition, the local modes can only be excited by phonons whose polarization vectors are not perpendicular to the Burgers vectors of dislocations. Recall that Anderson and coworkers [6,7] reported that "all measurements of thermal conductivity and ballistic phonon propagation in deformed LiF crystals are consistent with an interpretation in which the slow transverse (and possibly longitudinal) phonon mode is more strongly scattered by dislocations than the fast transverse mode". Mechanistically, this experimental observation is explained by the role of the shear stress component of the phonons along the Burgers vectors of dislocations in activating the out-of-phase local dislocation vibrational modes. In contrast to the speculation of Anderson and coworkers [6,7], no resonant interaction between LA phonons and dislocations has been observed in this work.

To explain the discrepancy between theory and experiment on thermal transport properties of LiF and other ionic materials, Taylor and coworkers suggested that the discrepancy may be due to "cooperative scattering by nonrandomly distributed dislocations" [11]. This work has demonstrated a clear pattern of

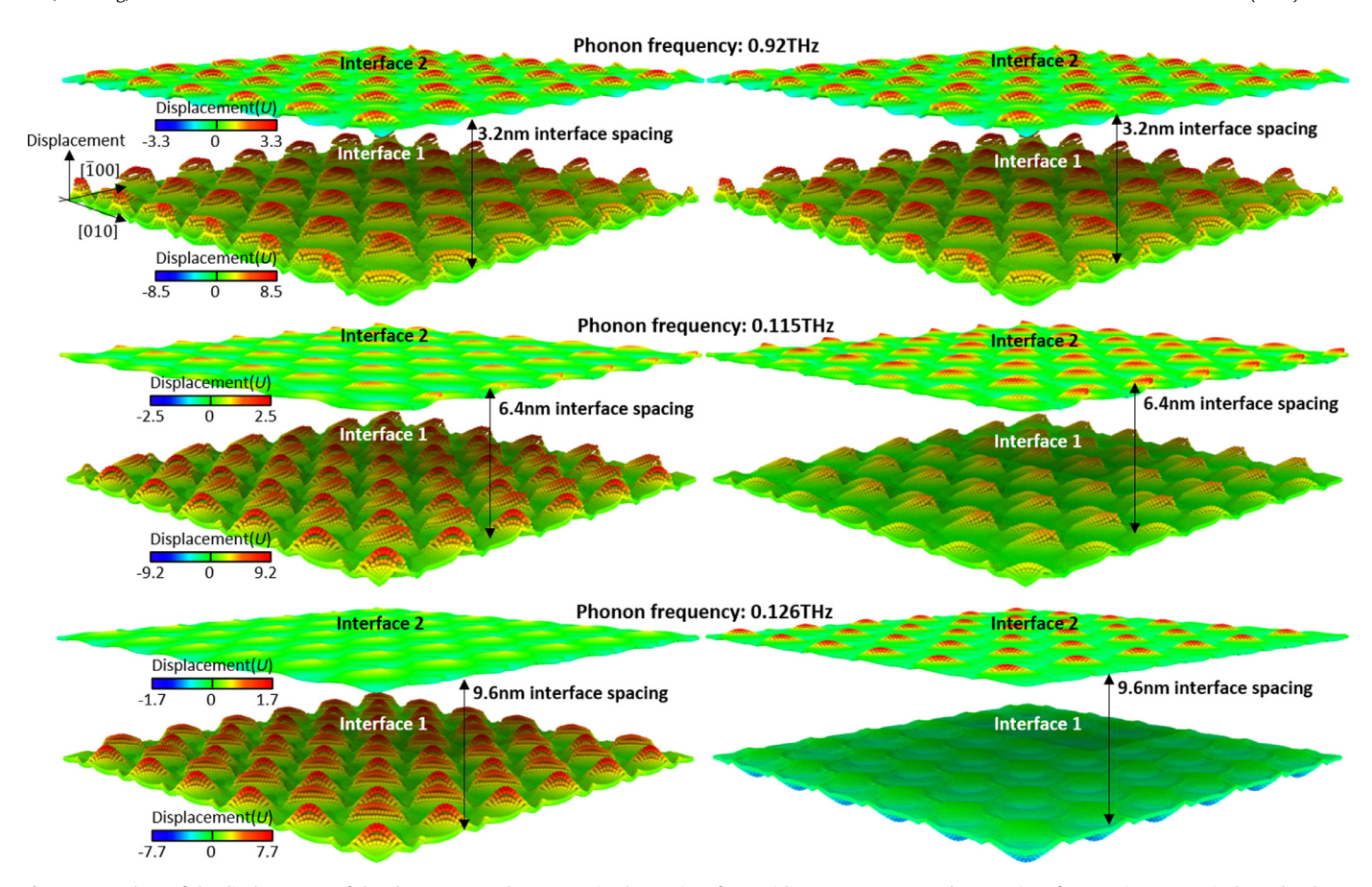


Fig. 14. Snapshots of the displacements of the PbSe atoms at the two semi-coherent interfaces with 3.2 nm, 6.4 nm, and 9.6 nm interface spacing, respectively, under the TA phonon pulses that lead to the strongest vibrations of the misfit dislocations, i.e., with frequencies of 0.92 THz, 0.115 THz, and 0.126 THz, respectively. Left (right) column: snapshots taken at the timestep when the misfit dislocations at the first (second) interface have the largest displacements.

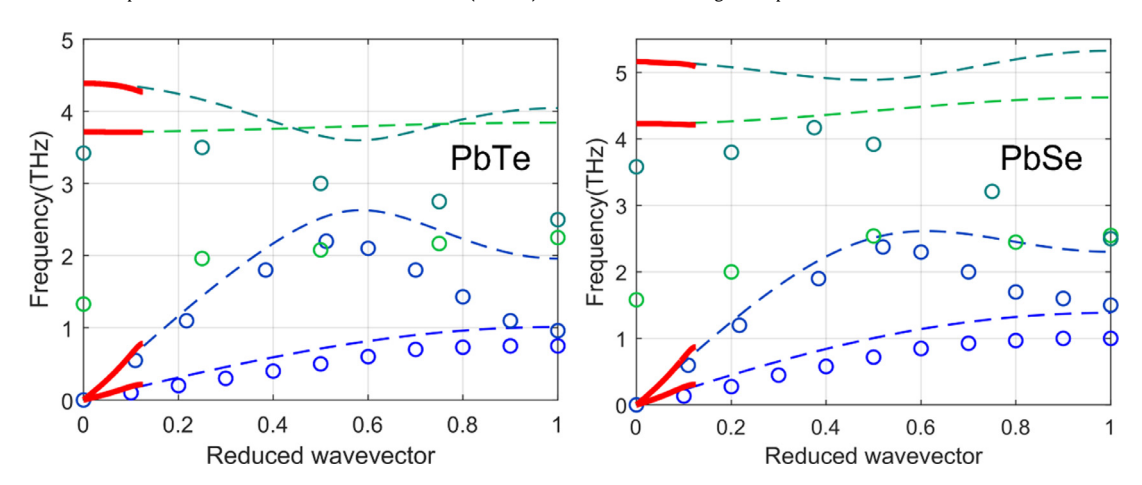


Fig. A.1. Phonon dispersion relations for PbTe (left) and PbSe (right) based on the empirical interatomic potential [24] employed in this work. The dashed dispersion curves are obtained via CAC using the finest mesh size, which are identical to that obtained by MD; the red solid curves are obtained via CAC using a uniform coarse finite element mesh with each element containing 1024 atoms; the circles are DFT calculations reported in ref. [59]. (For interpretation of the references to color in this figure legend, the reader is referred to the web version of this article.)

the motion of the misfit dislocation networks, in which the dislocations are shown to vibrate cooperatively, rather than randomly or independently, thus confirming the emergence of collective motion of dislocations. In addition, simulation results show that the dynamic properties of the misfit dislocation network localized within one interface can be changed by the presence of misfit dislocations at other interfaces, and this change depends on the spacing between the dislocation networks. More generally, this work supports the notion that the responses to

heat pulses can be significantly influenced by the collective interaction between phonons and the distribution of misfit dislocations, driven primarily by shear waves. Hence, it is demonstrated that CAC simulations can enhance quantitative understanding of the collective behavior of dislocations at interfaces. This suggests the utility of CAC for the simulation of acoustic metamaterials that derive their characteristics from mesoscopic arrangements, including the role of defect distributions in modifying dynamic response.

Declaration of Competing Interest

The authors declare that they have no known competing financial interests or personal relationships that could have appeared to influence the work reported in this paper.

Acknowledgments

This material is based on research supported by the US National Science Foundation as a collaborative effort under Award Numbers CMMI-1761512 (YL, ZZ, AD, and YC) and CMMI 1761553 (DLM). The work of YC is also partially supported by CMMI-2054607. The computer simulations are funded by the Extreme Science and Engineering Discovery Environment (XSEDE) allocation TG-DMR190008. We thank Dr. Zhaochuan Fan for the help with the interatomic potential.

Appendix A. Phonon dispersion relations of PbTe and PbSe

Fig. A.1.

References

- J.D. Eshelby, Dislocations as a cause of mechanical damping in metals, Proc. R. Soc. Lond. Ser. A 197 (1949) 396–416.
- [2] F.R.N. Nabarro, The interaction of screw dislocations and sound waves, Proc. R. Soc. Lond. Ser. A 209 (1951) 278–290.
- [3] A. Granato, Thermal properties of mobile defects, Phys. Rev. 111 (1958) 740.
- [4] R. Sproull, M. Moss, H. Weinstock, Effect of dislocations on the thermal conductivity of lithium fluoride, J. Appl. Phys. 30 (1959) 334–337.
- [5] P.G. Klemens, The scattering of low-frequency lattice waves by static imperfections, Proc. Phys. Soc. Sect. A 68 (1955) 1113–1128, doi:10.1088/0370-1298/68/12/303.
- [6] E.P. Roth, A.C. Anderson, Interaction between thermal phonons and dislocations in LiF, Phys. Rev. B 20 (1979) 768.
- [7] A. Anderson, M. Malinowski, Interaction between thermal phonons and dislocations in LiF, Phys. Rev. B 5 (1972) 3199.
- [8] J.S. Koehler, Imperfections in nearly perfect crystals, in: W. Shockley, J.H. Hollomon, R. Maurer, F. Seitz (Eds.), Acta Crystallographica, 5, 1952, p. 860, doi:10.1107/S0365110x52002677.
- [9] A. Granato, K. Lücke, Theory of mechanical damping due to dislocations, J. Appl. Phys. 27 (1956) 583–593.
- [10] J. Garber, A. Granato, Reradiation and viscous dislocation damping, J. Phys. Chem Solids 31 (1970) 1863–1867.
- [11] A. Taylor, H. Albers, R. Pohl, Effect of plastic deformation on the thermal conductivity of various ionic crystals, J. Appl. Phys. 36 (1965) 2270–2278.
- [12] G.A. Kneeze, A. Granato, Effect of independent and coupled vibrations of dislocations on low-temperature thermal conductivity in alkali halides, Phys. Rev. B 25 (1982) 2851.
- [13] G.A. Northrop, E.J. Cotts, A.C. Anderson, J.P. Wolfe, Anisotropic phonondislocation scattering in deformed LiF, Phys. Rev. B 27 (1983) 6395–6408, doi:10.1103/PhysRevB.27.6395.
- [14] Y. Sun, et al., Strong phonon localization in PbTe with dislocations and large deviation to Matthiessen's rule, npj Comput. Mater. 5 (2019) 1–6.
- [15] Y. Sun, et al., Molecular dynamics simulations of the effect of dislocations on the thermal conductivity of iron, J. Appl. Phys. 127 (2020) 045106.
- [16] D. Spiteri, J.W. Pomeroy, M. Kuball, Influence of microstructural defects on the thermal conductivity of Ga N: a molecular dynamics study, *Phys. Status Solidi* (b) 250 (2013) 1541–1545.
- [17] Y. Chen, Reformulation of microscopic balance equations for multiscale materials modeling, J. Chem. Phys. 130 (2009) 134706.
- [18] Y. Chen, J. Lee, Atomistic formulation of a multiscale field theory for nano/micro solids, Philos. Mag. 85 (2005) 4095–4126.
- [19] Y. Chen, S. Shabanov, D.L. McDowell, Concurrent atomistic-continuum modeling of crystalline materials, J. Appl. Phys. 126 (2019) 101101, doi:10.1063/1. 5099653.
- [20] D. Greig, Thermoelectricity and thermal conductivity in the lead sulfide group of semiconductors, Phys. Rev. 120 (1960) 358.
- [21] G. Springholz, K. Wiesauer, Nanoscale dislocation patterning in PbTe/PbSe (001) lattice-mismatched heteroepitaxy, Phys. Rev. Lett. 88 (2001) 015507.
- [22] K. Wiesauer, G. Springholz, Strain relaxation and dislocation patterning in PbTe/PbSe (001) lattice-mismatched heteroepitaxy, Appl. Surf. Sci. 188 (2002) 49-54
- [23] Z. Fan, et al., A transferable force field for CdS-CdSe-PbS-PbSe solid systems, J. Chem. Phys. 141 (2014) 244503.
- [24] Y. Li, Z. Fan, W. Li, D.L. McDowell, Y. Chen, A multiscale study of misfit dislocations in PbTe/PbSe(001) heteroepitaxy, J. Mater. Res. (2019) 1–9, doi:10.1557/ imr.2019.69.
- [25] H. Beyer, et al., PbTe based superlattice structures with high thermoelectric efficiency, Appl. Phys. Lett. 80 (2002) 1216–1218.

[26] Q. Zhang, et al., Heavy doping and band engineering by potassium to improve the thermoelectric figure of merit in p-type PbTe, PbSe, and PbTe_{1-y} Se_y, J. Am. Chem. Soc. 134 (2012) 10031–10038.

- [27] Y. Chen, A. Diaz, Physical foundation and consistent formulation of atomic-level fluxes in transport processes, Phys. Rev. E 98 (2018) 052113.
- [28] Y. Chen, A. Diaz, Local momentum and heat fluxes in transient transport processes and inhomogeneous systems, Phys. Rev. E 94 (2016) 053309.
- [29] A. Diaz, D. Davydov, Y. Chen, On the equivalence of the two foundational formulations for atomistic flux in inhomogeneous transport processes, Proc. R. Soc. A 475 (2019) 20180688
- [30] Chen, Y. The origin of the distinction between microscopic formulas for stress and Cauchy stress. *EPL (Europhys. Lett.)*116, 34003 (2016).
- [31] A. Diaz, et al., A parallel algorithm for the concurrent atomistic-continuum methodology, J. Comput. Phys. (2022) 111140, doi:10.1016/j.jcp.2022.111140.
- [32] Q. Deng, L. Xiong, Y. Chen, Coarse-graining atomistic dynamics of brittle fracture by finite element method, Int. J. Plast. 26 (2010) 1402–1414.
- [33] Q. Deng, Y. Chen, A coarse-grained atomistic method for 3D dynamic fracture simulation, J. Multiscale Comput. Eng. 11 (2013) 227–237.
- [34] L. Xiong, Y. Chen, Coarse-grained simulations of single-crystal silicon, Model. Simul. Mater. Sci. Eng. 17 (2009) 035002.
- [35] L. Xiong, Q. Deng, G. Tucker, D.L. McDowell, Y. Chen, A concurrent scheme for passing dislocations from atomistic to continuum domains, Acta Mater. 60 (2012) 899–913.
- [36] L. Xiong, G. Tucker, D.L. McDowell, Y. Chen, Coarse-grained atomistic simulation of dislocations, J. Mech. Phys. Solids 59 (2011) 160–177.
- [37] S. Yang, L. Xiong, Q. Deng, Y. Chen, Concurrent atomistic and continuum simulation of strontium titanate, Acta Mater. 61 (2013) 89–102.
- [38] L. Xiong, et al., Coarse-grained elastodynamics of fast moving dislocations, Acta Mater. 104 (2016) 143–155.
- [39] L. Xiong, Q. Deng, G.J. Tucker, D.L. McDowell, Y. Chen, Coarse-grained atomistic simulations of dislocations in Al, Ni and Cu crystals, Int. J. Plast. 38 (2012) 86–101.
- [40] L. Xiong, D.L. McDowell, Y. Chen, Nucleation and growth of dislocation loops in Cu, Al and Si by a concurrent atomistic-continuum method, Scr. Mater. 67 (2012) 633–636.
- [41] S. Xu, L. Xiong, Y. Chen, D.L. McDowell, Edge dislocations bowing out from a row of collinear obstacles in Al, Scr. Mater. 123 (2016) 135–139.
- [42] S. Xu, L. Xiong, Y. Chen, D.L. McDowell, An analysis of key characteristics of the frank-read source process in FCC metals, J. Mech. Phys. Solids 96 (2016) 460–476.
- [43] S. Xu, L. Xiong, Y. Chen, D.L. McDowell, Sequential slip transfer of mixed-character dislocations across Σ3 coherent twin boundary in FCC metals: a concurrent atomistic-continuum study, npj Comput. Mater. 2 (2016) 15016.
- [44] L. Xiong, S. Xu, D.L. McDowell, Y. Chen, Concurrent atomistic-continuum simulations of dislocation-void interactions in fcc crystals, Int. J. Plast. 65 (2015) 22 degrees of the continuum simulations of dislocation-void interactions in fcc crystals, Int. J. Plast. 65 (2015)
- [45] S. Xu, L. Xiong, Y. Chen, D.L. McDowell, Shear stress-and line length-dependent screw dislocation cross-slip in FCC Ni, Acta Mater. 122 (2017) 412–419.
- [46] S. Xu, L. Xiong, Y. Chen, D.L. McDowell, Validation of the concurrent atomistic-continuum method on screw dislocation/stacking fault interactions, Crystals 7 (2017) 120.
- [47] S. Yang, Y. Chen, in: Multiscale Materials Modeling for Nanomechanics, Springer International Publishing, 2016, pp. 261–296.
- [48] S. Yang, Y. Chen, Concurrent atomistic and continuum simulation of bi-crystal strontium titanate with tilt grain boundary, Proc. R. Soc. A 471 (2015).
- [49] S. Yang, N. Zhang, Y. Chen, Concurrent atomistic-continuum simulation of polycrystalline strontium titanate, Philos. Mag. 95 (2015) 2697–2716.
- [50] X. Chen, L. Xiong, D.L. McDowell, Y. Chen, Effects of phonons on mobility of dislocations and dislocation arrays, Scr. Mater. 137 (2017) 22–26, doi:10.1016/j. scriptamat.2017.04.033.
- [51] L. Xiong, D.L. McDowell, Y. Chen, Sub-THz phonon drag on dislocations by coarse-grained atomistic simulations, Int. J. Plast. 55 (2014) 268–278.
- [52] X. Chen, et al., Ballistic-diffusive phonon heat transport across grain boundaries, Acta Mater. 136 (2017) 355–365, doi:10.1016/j.actamat.2017.06.054.
- [53] Y. Li, A. Diaz, X. Chen, D.L. McDowell, Y. Chen, Interference, scattering, and transmission of acoustic phonons in Si phononic crystals, Acta Mater. 224 (2022) 117481.
- [54] T. Zhu, C.-y. Wang, Misfit dislocation networks in the γ/γ' phase interface of a Ni-based single-crystal superalloy: molecular dynamics simulations, Phys. Rev. B 72 (2005) 014111.
- [55] S. Yang, A Concurrent Atomistic-Continuum Method For Simulating Defects in Ionic Materials, University of Florida, 2014.
- [56] X. Zhou, et al., Stillinger-weber potential for the II-VI elements Zn-Cd-Hg-S-Se-Te, Phys. Rev. B 88 (2013) 085309.
- [57] D.K. Ward, X.W. Zhou, B.M. Wong, F. Doty, J Zimmerman, Analytical bond-order potential for the cadmium telluride binary system, Phys. Rev. B 85 (2012) 115206.
- [58] K. Wiesauer, G. Springholz, Near-equilibrium strain relaxation and misfit dislocation interactions in PbTe on PbSe (001) heteroepitaxy, Appl. Phys. Lett. 83 (2003) 5160-5162.
- [59] J.M. Skelton, S.C. Parker, A. Togo, I. Tanaka, A. Walsh, Thermal physics of the lead chalcogenides PbS, PbSe, and PbTe from first principles, Phys. Rev. B 89 (2014) 205203.
- [60] P. Schapotschnikow, M.A. Van Huis, H.W. Zandbergen, D. Vanmaekelbergh, T.J.H. Vlugt, Morphological transformations and fusion of PbSe nanocrystals studied using atomistic simulations, Nano Lett. 10 (2010) 3966–3971.

[61] H. Kim, M Kaviany, Effect of thermal disorder on high figure of merit in PbTe, Phys. Rev. B 86 (2012) 045213.

- [62] Qiu, B., Bao, H., Ruan, X., Zhang, G. & Wu, Y. 659–670 (American Society of Mechanical Engineers). 2022
- [63] G. Patriarche, F. Jeannes, J.L. Oudar, F. Glas, Structure of the GaAs/InP interface obtained by direct wafer bonding optimised for surface emitting optical devices, J. Appl. Phys. 82 (1997) 4892–4903.
- [64] A. Stukowski, K. Albe, Extracting dislocations and non-dislocation crystal defects from atomistic simulation data, Model Simul. Mater. Sci. Eng. 18 (2010) 085001
- [65] P.K. Schelling, S.R. Phillpot, P. Keblinski, Phonon wave-packet dynamics at semiconductor interfaces by molecular-dynamics simulation, Appl. Phys. Lett. 80 (2002) 2484–2486, doi:10.1063/1.1465106.
- [66] Y. Li, et al., Phonon spectrum and phonon focusing in coarse-grained atomistic simulations, Comput. Mater. Sci. 162 (2019) 21–32, doi:10.1016/j.commatsci. 2019.02.020.

- [67] X. Chen, A. Diaz, L. Xiong, D.L. McDowell, Y. Chen, Passing waves from atomistic to continuum, J. Comput. Phys. 354 (2018) 393–402, doi:10.1016/j.jcp.2017. 10.038.
- [68] R. Landauer, Spatial variation of currents and fields due to localized scatterers in metallic conduction, IBM J. Res. Dev. 1 (1957) 223–231.
- [69] J.S. Wang, J. Wang, J.T. Lü, Quantum thermal transport in nanostructures, Eur. Phys. J. B 62 (2008) 381–404.
- [70] E.S. Landry, A.J.H. McGaughey, Thermal boundary resistance predictions from molecular dynamics simulations and theoretical calculations, Phys. Rev. B 80 (2009) 165304.
- [71] T. Tadano, Y. Gohda, S. Tsuneyuki, Anharmonic force constants extracted from first-principles molecular dynamics: applications to heat transfer simulations, J. Phys. 26 (2014) 225402.
- [72] T. Ninomiya, Dislocation vibration and phonon scattering, J. Phys. Soc. Jpn. 25 (1968) 830–840.